THE JOURNAL OF BIOLOGICAL CHEMISTRY VOL. 286, NO. 34, pp. 29904–29912, August 26, 2011

Effect of Src Kinase Phosphorylation on Disordered C-terminal Domain of *N*-Methyl-D-aspartic Acid (NMDA) Receptor Subunit GluN2B Protein*[S]

Received for publication, May 6, 2011, and in revised form, June 17, 2011 Published, JBC Papers in Press, June 28, 2011, DOI 10.1074/jbc.M111.258897

Ucheor B. Choi[‡], Shifeng Xiao[§], Lonnie P. Wollmuth[¶], and Mark E. Bowen[‡1]

From the Departments of [‡]Physiology and Biophysics, [§]Chemistry, and [¶]Neurobiology and Behavior, Stony Brook University, Stony Brook, New York 11794

NMDA receptors are ligand-gated ion channels with a regulatory intracellular C-terminal domain (CTD). In GluN2B, the CTD is the largest domain in the protein but is intrinsically disordered. The GluN2B subunit is the major tyrosine-phosphorylated protein in synapses. Src kinase phosphorylates the GluN2B CTD, but it is unknown how this affects channel activity. In disordered proteins, phosphorylation can tip the balance between order and disorder. Transitions can occur in both directions, so it is not currently possible to predict the effects of phosphorylation. We used single molecule fluorescence to characterize the effects of Src phosphorylation on GluN2B. Scanning fluorescent labeling sites throughout the domain showed no positional dependence of the energy transfer. Instead, efficiency only scaled with the separation between labeling sites suggestive of a relatively featureless conformational energy landscape. Src phosphorylation led to a general expansion of the polypeptide, which would result in greater exposure of known protein-binding sites and increase the physical separation between contiguous sites. Phosphorylation makes the CTD more like a random coil leaving open the question of how Src exerts its effects on the NMDA receptor.

Ionotropic glutamate receptors are central to mediating the plasticity that underlies higher brain functions like learning and memory and development of neural circuits (1). NMDA-sensitive glutamate receptors (NMDAR)[2] are ligand-gated ion channels with modular functional components that include extracellular N-terminal and ligand-binding domains, a transmembrane ion channel, and a regulatory intracellular C-terminal domain (CTD) (Fig. 1*A*) (2). Although one can measure ligand-gated channel activity without the CTD (3), it is central to NMDAR regulation in neurons. The CTD regulates membrane expression and synaptic clustering (1, 4), alters gating and ion selectivity of the channel pore (2), and acts as a scaffold for intracellular signaling molecules (*e.g.* Ca^{2+}/calmodulin-dependent kinase 2 (CAMKII)). The activity of the CTD in these different functional roles depends on the state of post-translational modifications (2), but we lack a mechanism to describe how the CTD influences the ligand-gated channel.

NMDARs are obligate heterotetramers being composed of the ubiquitous GluN1 subunit and some combination of GluN2 and/or GluN3 subunits. In the cortex, NMDARs typically contain GluN2A or GluN2B subunits (5). In GluN2A and GluN2B, the CTD is the largest single domain in the protein (Fig. 1*A*) (6). Genetic deletion of the GluN2B CTD is lethal (7), which is equivalent to deleting the entire receptor (8).

The CTD allows many signaling pathways to modulate GluN2B. A central palmitoylation motif divides the CTD into two "domains" (CTD1 and CTD2, Fig. 1*B*) (9). This lipid modification would drive the N-terminal membrane attachment of CTD2 (10), and it affects trafficking and synaptic localization of NMDARs (9). The CTD also interacts with scaffold proteins that direct trafficking and synaptic retention (11–13).

The GluN2B CTD is the target of multiple kinases (14) and the major tyrosine-phosphorylated protein in the postsynaptic density (15). Somehow phosphorylation near the distal C terminus affects the ion channel. For example, phosphorylation by Src family tyrosine kinases enhances NMDAR currents (16, 17) and reduces Zn^{2+} inhibition (18, 19).

The CTD of GluN2B is predicted to be intrinsically disordered by both PONDR (20) and IUPRED (Fig. 1*B*) (21). Intrinsically disordered proteins lack fixed secondary or tertiary structure and instead dynamically sample an ensemble of different conformations (22). Phosphorylation sites are frequently located in disordered regions, even in proteins with structured domains (23). Phosphorylation can promote structural transitions between order and disorder (24). Structure can be induced in disordered regions (25) or structure can be lost (26). Phosphorylation can reduce tertiary contacts (27) or increase intramolecular dynamics (26) within the native state ensemble. Increasing the charge of disordered peptides can favor more extended states (28–30). However, some proteins show no global expansion upon phosphorylation (31).

Recently, we provided the first experimental confirmation of disorder in CTD2 (Fig. 1*B*) from GluN2B (32). However, CTD2 does not show the rapid intramolecular dynamics of a random coil but rather undergoes conformational switching on the second time scale (32). If the structure dictates function then the function would be changing every second. Switching would

* This work was supported, in whole or in part, by National Institutes of Health Grants MH081923 (to M. E. B.) and MH066892 (to L. P. W.). This work was also supported by a National Research Service Award (to U. B. C.).

[S] The on-line version of this article (available at http://www.jbc.org) contains supplemental Figs. S1 and S2.

[1] To whom correspondence should be addressed: Dept. of Physiology and Biophysics, BST 5-121, Stony Brook University, Stony Brook, NY 11794-8661. E-mail: mark.bowen@sunysb.edu.

[2] The abbreviations used are: NMDAR, NMDA receptor; CTD, C-terminal domain; SEC, size exclusion chromatography; smFRET, single molecule FRET.

allow "conformational selection," wherein a productive interaction could only occur if the active conformation is present when the ligand arrives (33).

In this study, we describe the effect of Src phosphorylation on CTD2 from the GluN2B subunit, which contains both physiological Src sites (Tyr-1336 and Tyr-1472). Single molecule fluorescence measurements showed no positional dependence of the fluorescence resonance energy transfer (FRET) efficiency. Instead, FRET only scaled with the separation between labeling sites suggesting a lack of local structure.

Phosphorylation led to a general expansion of the polypeptide rather than inducing stable structure. Expansion would result in greater exposure of potential protein-binding sites, which could change interactions within the receptor or with other synaptic proteins. Phosphorylation did not stabilize an "active" conformation instead making the CTD more random coil-like. How the CTD affects channel function remains an open question.

EXPERIMENTAL PROCEDURES

Protein Expression and Purification—The C-terminal domain 2 of GluN2B (residues 1259–1482, Fig. 1*B*) was cloned into pPROEX HTB (Invitrogen) and expressed in the Rosetta strain of *Escherichia coli* (EMD Biosciences, San Diego). The His_6 fusion was purified under reducing and denaturing conditions as described (32). The protein was exchanged to nondenaturing conditions by extensive washing while bound to nickel-nitrilotriacetic acid-agarose. The His_6 tag was removed with tobacco etch virus protease, and the protein was further purified with cation exchange and size exclusion (GE Healthcare). Chicken c-Src kinase (residues 83–534) was kindly provided by Dr. Markus Seeliger. Proteins were phosphorylated in the presence of 1 mM ATP and 1 mM $MgCl_2$ followed by cation exchange to remove Src.

Limited Proteolysis—Wild-type CTD2 was purified and phosphorylated as described above. Sequencing grade trypsin and chymotrypsin were added at 0.002 mg/ml (Promega, Madison, WI). Replicate samples were prepared for each time point and inhibited at the indicated time with 0.5 mM phenylmethylsulfonyl fluoride (PMSF).

Circular Dichroism Spectroscopy—Circular dichroism (CD) spectra were collected using a Chirascan CD spectrometer (Applied Photophysics, Leatherhead, UK at 0.2 mg/ml protein concentration in PBS (10 mM sodium phosphate, 50 mM NaCl, 0.5 mM DTT, pH 7.4) at 20 °C. The step size was 1 nm, and the signal averaging time was 0.3 s.

Analytical Size Exclusion Chromatography—Purified proteins were injected onto a Shodex KW-802.5 column in 20 mM Tris, 150 mM NaCl, 0.5 mM DTT, pH 7.5, at 4 °C as described (32). Radius of hydration was determined using a calibration based on the molecular weight of gel filtration standards (Bio-Rad) and the published relationship for globular proteins ($\log(R_H) = -0.204 + 0.357 \log(M_r)$) (22). This allows us to estimate R_H based on elution time.

Single Molecule Microscopy—Single molecule experiments were performed as described (32, 34). Briefly, proteins were fluorescently labeled with an equimolar ratio of Alexa 555 and 647 maleimide (Invitrogen). Ensemble fluorometry to characterize labeling sties was as described (34). Proteins were encapsulated in egg phosphatidylcholine liposomes (containing 0.1 mol % of biotin-phosphatidylethanolamine) by extrusion (Avanti Polar Lipids, Alabaster, AL). Liposomes were immobilized on a quartz microscope slide coated with biotinylated BSA and streptavidin.

Emission signals were recorded in a prism-type total internal reflection microscope, detected by an iXon EMCCD (Andor Technologies, Belfast, UK) and illuminated by an alternating laser sequence of 635 and 532 nm to distinguish proteins labeled with two donor dyes, two acceptor dyes, and exactly 1 donor and 1 acceptor dye. Representative traces are shown in supplemental Fig. S1. FRET efficiency (E) is calculated from the background subtracted intensity of acceptor (I_A) and donor (I_D) emission as shown in Equation 1,

$$E = \frac{I_A}{I_A + I_D} \quad \text{(Eq. 1)}$$

Biotinylation for Surface Immobilization—Proteins were biotinylated during recombinant expression in the AVB101 strain of *E. coli* that expresses biotin ligase (Avidity, Aurora, CO). Constructs were cloned into a modified version of pPROEX HTB that appends a consensus biotinylation sequence (GSGLNDIFEANKIEWHE) to the N terminus of CTD2. The tag is C-terminal to the tobacco etch virus cleavage site so biotin remains after the His_6 tag is removed. Biotinylated proteins behaved similarly during chromatography and fluorescent labeling and were robustly phosphorylated by recombinant Src.

To avoid nonspecific adsorption to the quartz microscope slide, we first coated the surface with biotinylated BSA. BSA alone is a poor surface passivation for proteins as levels of nonspecific binding remain high (supplemental Fig. S2*A*). BSA is a fatty acid-binding protein that is capable of hydrophobic interactions. To minimize nonspecific interactions, the BSA surface was exposed to a dilute solution of protein-free egg phosphatidylcholine liposomes (1 mg/ml). The resultant surface displays very low levels of nonspecific binding (supplemental Fig. S2*B*). Finally, a 0.1 mg/ml solution of streptavidin is added to create specific attachment sites for labeled proteins (supplemental Fig. S2*C*). Labeled proteins show negligible binding to this surface in the absence of biotinylation (supplemental Fig. S2*D*). Experimental details of data collection and analysis were identical to encapsulation studies.

RESULTS

Constructs Used in This Study—The CTD of the GluN2B subunit contains two palmitoylation sites, which are dynamically modified in neurons (9). The second palmitoylation site (Cys cluster II, residues Cys-1215 to Cys-1245) divides the CTD into two halves, which we have termed CTD1 and CTD2 (Fig. 1*B*). CTD2 could be purified under nondenaturing conditions indicating that the protein is not expressed in inclusion bodies (data not shown). CTD2 was prone to degradation during the purification, which could be removed by size exclusion. We lysed the cells in denaturants to avoid this complication and "refolded" the protein by exchanging to physiological buffer while bound to beads. Measurements on denaturant and native

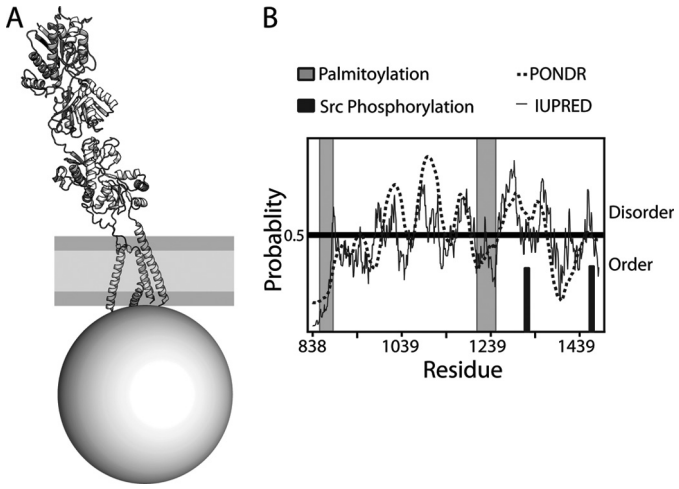

FIGURE 1. **Disorder in the C-terminal domain of GluN2B.** *A,* known and unknown portions of the glutamate receptor structure. A schematic representation of the x-ray structure of an AMPA-sensitive glutamate receptor subunit (3KG2) (38) is depicted within a membrane (*gray*). The disordered C-terminal domain is drawn in approximate scale (*circle*). The CTD volume was calculated based on the assumption of a compact disordered globule (22), which is supported by our data. *B,* prediction of intrinsic disorder in the CTD. Probability of disorder is plotted for residues 838–1482. We analyzed the CTD with two major disorder predictors PONDR (*dashed line*) (20) and IUPRED (*solid line*) (21). Plot shows probability of disorder for each residue. The location of the palmitoylation sites is indicated by the *gray vertical bars* crossing the panel. The second palmitoylation site defines an intervening membrane binding region that partitions the CTD into two domains that we term CTD1 and CTD2. The location of the phosphorylation sites are inset at the bottom of the panel as *black vertical bars*.

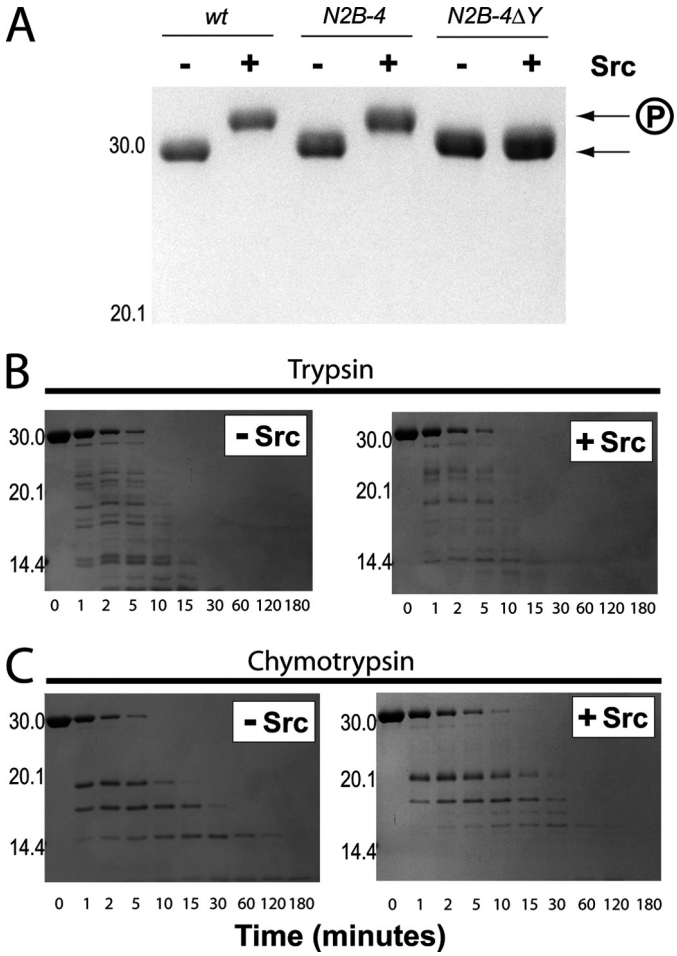

FIGURE 2. **Src phosphorylation increases protease sensitivity of the GluN2B CTD2.** *A,* effect of Src phosphorylation on the electrophoretic mobility of CTD2 during SDS-PAGE. Equal amounts of untreated and Src phosphorylated proteins were loaded on a 15% acrylamide gel. Position of the molecular weight markers is indicated to the *left* of the panel. For each sample, the *1st lane* is untreated (−), and the *2nd lane* has been phosphorylated (+). As indicated by the *arrows* to the *right* of the panel, phosphorylation decreased the apparent electrophoretic mobility. Representative samples of wild type CTD2, N2B-4, and N2B-4 ΔY, which lack the tyrosine phosphorylation sites (Y1336T and Y1472C) (Fig. 4*A* and Table 1), are shown, but all samples showed a similar shift, which was taken as diagnostic of phosphorylation. *B,* effect of phosphorylation on limited proteolysis of CTD2 by trypsin. *Left,* GluN2B wild type CTD2 was exposed to 0.002 mg/ml trypsin for the indicated time (minutes) before the addition of PMSF to stop the reaction. *Right,* same sample was Src-phosphorylated before the addition of protease. Position of the molecular weight markers is indicated to the *left* of the panel. *C,* effect of phosphorylation on limited proteolysis of CTD2 by chymotrypsin. *Left,* GluN2B wild type CTD2 was exposed to 0.002 mg/ml chymotrypsin for the indicated time (minutes) before the addition of PMSF to stop the reaction. *Right,* same sample was Src phosphorylated before the addition of protease. Position of the molecular weight markers is indicated to the *left* of the panel.

purified proteins were identical indicating that the use of denaturants is not causing the intrinsic disorder (data not shown). All measurements were made in biological buffers at physiological pH with sodium chloride. Although these are not the physiological counter ions for intracellular proteins, measurements made in a range of counter ions showed little difference at physiological ionic strengths (data not shown).

Ensemble Characterization of CTD2 Phosphorylation—Nakazawa *et al.* (35) demonstrated in 2001 that Src robustly phosphorylates recombinant GluN2B CTD constructs *in vitro*. To phosphorylate CTD2, we used purified recombinant c-Src (residues 83–534), which contains Src homology 2 and 3 and kinase domains. SDS-PAGE was used to confirm phosphorylation of all constructs. CTD2 is 24.9 kDa but runs anomalously on SDS-PAGE, coincident with the 30-kDa marker (Fig. 2*A*). Src phosphorylation of CTD2 induced a discernible decrease in the electrophoretic mobility on SDS-PAGE (*lanes marked* +, Fig. 2*A*). The shift from phosphorylation was dependent on the presence of Mg^{2+} as Src in the presence of ATP alone had no effect. To confirm the sites of Src phosphorylation, we mutated Tyr-1336 and Tyr-1472 to threonine (ΔY), which eliminated the mobility shift induced by Src (*right lanes,* Fig. 2*A*).

Limited trypsin proteolysis of CTD2 with 2 μg/ml trypsin resulted in complete degradation in less than 30 min as expected for a disordered protein (Fig. 2*B*). High molecular weight intermediate bands are visible at early time points indicating that some cleavage sites are partially protected. CTD2 is degraded more slowly by chymotrypsin with clear protected intermediates lasting close to 2 h (Fig. 2*C*). This suggests differential exposure of lysine and arginine residues (trypsin) relative to aromatic residues (chymotrypsin).

Phosphorylation did not alter the kinetics of digestion of CTD2 by either protease. However, the structural changes induced by phosphorylation altered the pattern of digestion. This is seen in the loss of most of the intermediate bands in the trypsin digestion, indicating greater exposure of cleavage sites (Fig. 2*B*). Similarly, phosphorylation also changed the digestion pattern for chymotrypsin (Fig. 2*C*). In particular, the ~14 kDa band is destabilized after phosphorylation, and a new higher molecular weight band appears ~17 kDa. All intermediate

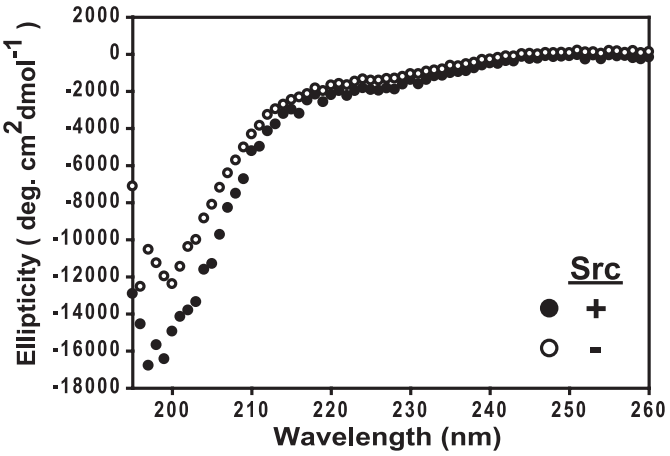

FIGURE 3. **Phosphorylation does not induce secondary structure in the GluN2B CTD2.** Near UV circular dichroism spectra of wild type CTD2 from GluN2B. Spectrum for the unphosphorylated protein is shown as *open circles*. Spectrum for the Src-phosphorylated protein is shown as *filled circles*. Data are plotted as molar ellipticity as the proteins are identical aside from the phosphotyrosine. Spectra were recorded in 10 mM phosphate, 50 mM NaCl at pH 7.5.

digestion products are shifted toward higher molecular weight indicating that the phosphorylation sites are present in these products.

To identify any changes in secondary structure, we used circular dichroism (Fig. 3). The spectrum for CTD2 shows no double minima at 208 and 222 nm indicating a lack of stable α-helices (*open circles,* Fig. 3). The negative peak at 200 nm is consistent with intrinsic disorder, but the slightly negative ellipticity above 210 nm suggests some β-sheet character. Phosphorylation had little effect on the CD spectrum (*filled circles,* Fig. 3) indicating that Src phosphorylation does not induce secondary structure in CTD2.

To measure the ensemble radius of hydration (R_H) we used analytical size exclusion chromatography (SEC). As in SDS-PAGE, CTD2 elutes from SEC with a much larger apparent molecular weight (78.8 $\pm$ 1 kDa). The calculated R_H value of 3.5 $\pm$ 0.02 nm for wild type CTD2 was consistent with a compact globular form of disorder rather than an extended random coil (22). Src phosphorylation increased the R_H of wild type CTD2 by 10% (to 3.9 $\pm$ 0.02 nm) suggesting that the negatively charged phosphate moieties are causing the polypeptide to expand. This is surprising because, based on the amino acid sequence, the net charge of CTD2 is +9, so phosphorylation actually reduces the net charge.

A 10% increase in R_H corresponds to a 30% increase in the effective volume occupied by the same amount of polypeptide, which implies much greater solvent exposure of the core. A folded protein of this size would have a R_H of only ~2.3 nm, which results in a much higher packing density. After phosphorylation, the measured R_H for CTD2 is close to that predicted for a random coil of the same molecular weight (4.1 nm) (22).

Single Molecule FRET Characterization of CTD2 Phosphorylation—We created a series of CTD2 constructs containing two unique cysteines for fluorescent labeling (Fig. 4*A*). The natural cysteine residues were used in some FRET pairs and are denoted by a capital C (*e.g.* C1394 in Table 1). Six other sites encoding for serine or threonine were chosen and mutated to cysteine (Table 1). To measure the conformation with FRET, we created eight double cysteine mutants based on these nine single labeling sites (Fig. 4*A*). We used SEC to confirm that neither the mutations nor fluorescent labeling affected the ensemble R_H. The mean R_H for the labeling mutants was 3.3 $\pm$ 0.1 nm without dyes and 3.2 $\pm$ 0.1 nm after labeling. After phosphorylation, the mean R_H for the labeling mutants was 3.9 $\pm$ 0.1 nm without dyes and 3.8 $\pm$ 0.1 nm after labeling. In contrast to the large increase in R_H induced by phosphorylation, the introduction of dyes has comparatively little effect.

To confirm that selected labeling sites did not affect photophysical properties of the dyes, we made ensemble measurements of donor anisotropy, which showed little difference from free dye (data not shown). Similarly, the donor quantum yield varied by less than 20% between sites (data not shown). Despite this finding, we are hesitant to interpret the FRET changes a distance given the following: 1) the uncertainty in relationship between the dye and the protein backbone and 2) the uncertainty of an appropriate model for the underlying dynamics.

Overlapping labeling site pairs were created to fully sample all of CTD2 in an effort to reveal any local structure (Fig. 4*A*). Samples were numbered in order with the increasing separation between labeling sites (Table 1). Data from single molecules containing a validated single donor and single acceptor dye pair were recorded at 100 ms/frame (Fig. 4*B*). The background corrected FRET was calculated for each frame of the movie (*i.e.* point wise) until photobleaching occurred (10–100 s). Histograms contain hundreds of single molecules and were replicated in separate experiments. In contrast to the narrow gaussian smFRET distribution of a random coil (32), all the labeling combinations showed broad distributions spanning the range of middle FRET values (Fig. 4*C*). Although the constructs sample different regions of CTD2, there was little dispersion in the FRET peaks suggesting a lack of local structure.

After Src phosphorylation (of fluorescently labeled protein), all labeling constructs showed a trend toward lower FRET values in the smFRET distributions (Fig. 5*A*, *solid curves*). Only three of the samples (NRB-3, -4, and -8) showed a statistically significant decrease in median FRET (Table 2). The different constructs are variably located relative to the phosphotyrosines (Fig. 4*A*) but show the same effect. The dyes did not affect Src phosphorylation as an identical electrophoretic mobility shift was induced in labeled protein (data not shown).

We plotted the median FRET value for the predominant peak in each histogram against the number of amino acids separating the labeling sites (Fig. 5*B*). FRET in CTD2 showed a simple linear dependence on the separation (Fig. 5*B*, *open circles*). The different constructs sampled regions throughout the protein but revealed this simple dependence rather than positional differences in the conformation of CTD2. After phosphorylation, the median FRET remained a linear function of the separation with a nearly identical slope to unphosphorylated CTD2 (Fig. 5*B*, *solid squares*). However, the intercept of the line had shifted toward a lower FRET. Even after phosphorylation, the median FRET values were much higher than expected for an extended random coil (32).

Phosphorylation did not have any effect on slow conformational dynamics in CTD2 (supplemental Fig. S1). All labeling

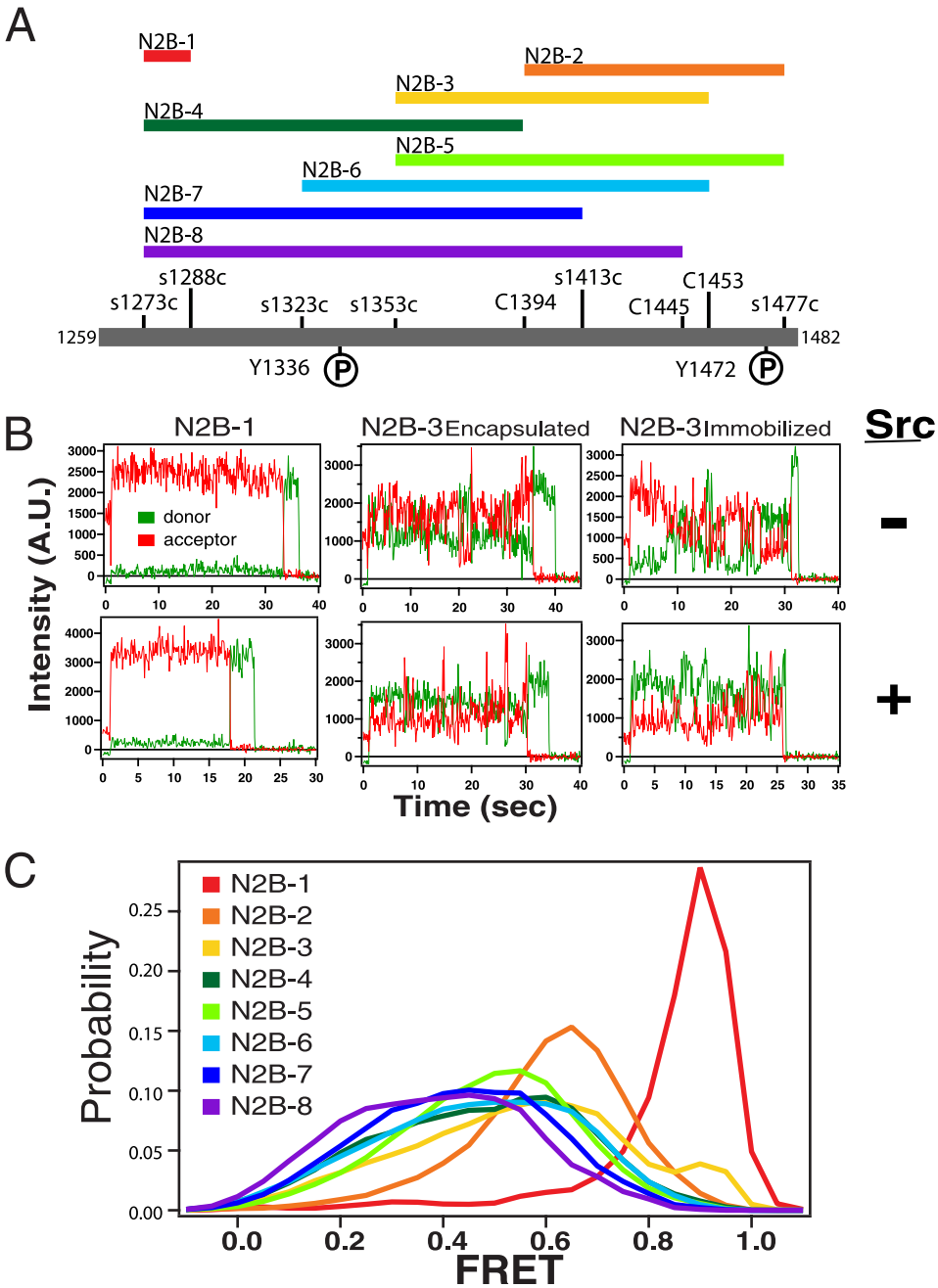

FIGURE 4. **Single molecule FRET measurements of the GluN2B CTD2 conformation.** *A,* constructs used in this experiment. Eight constructs of CTD2 were created that contained two unique cysteines for fluorescent labeling. Constructs were numbered in order of their fluorophore separation with NRB-1 being the shortest at 15 residues and NRB-8 being the longest at 172 residues (Table 1). The length and position of each construct are depicted as a *bar* above a scale representation of the primary sequence. The constructs overlap to sample the length of the polypeptide. The positions of cysteine residues used for labeling are indicated above the *scale bar*. Natural cysteines are indicated by *capitalization*. Phosphorylation sites are depicted below the *scale bar*. *B,* representative single molecule intensity time traces for unphosphorylated CTD2 (*top row*) and phosphorylated CTD2 (*bottom row*). Acceptor emission intensity is colored *red*. Donor emission intensity is colored *green*. Panels in the *left column* show representative single molecule intensity time traces for the control sample N2B-1 measured using the encapsulation method. Panels in the *middle* and *right columns* show representative single molecule intensity time traces of N2B-3 using the encapsulation and surface immobilization method, respectively. Additional representative data for the remaining samples are shown in supplemental Fig. S1. *C, histograms* of single molecule FRET for the eight labeling site combinations in CTD2. The *histogram* contains FRET values calculated for each 100 ms frame of observation. *Histograms* contain hundreds of molecules and were replicated in separate experiments. FRET is presented as normalized probability. *Histograms* are colored from *red* to *violet* in order of increasing fluorophore separation. N2B-1, *red*; N2B-2, *orange*; N2B-3, *yellow*; N2B-4, *dark green*; NRB-5, *light green*; N2B-6, *cyan*; N2B-7, *blue*; and N2B-8, *violet*.

constructs showed stochastic changes in FRET efficiency. As done previously (32), we characterized the FRET transitions using a Canny edge detection method (36). All constructs had a similar transition frequency in the range of 0.5 to 0.8 s^{-1} (data not shown). The transitioning was independent of the fluorophore separation and not affected by phosphorylation (Table 3).

The one exception was NRB-1, which showed a narrow FRET peak that was not shifted by phosphorylation, and it did not show stochastic changes in FRET efficiency. NRB-1 has

only 15 residues between labeling sites so high FRET is expected for such a short dye separation. This short polypeptide segment should not be capable of large conformational changes and is N-terminal to both phosphotyrosines. That we do not see FRET transitions or shifts confirms that these phenomena arise from CTD2 structural dynamics and not photophysics of the dye pair.

Effect of Surface Tethering on smFRET in CTD2—In the GluN2B subunit, CTD2 would be anchored to a lipid bilayer via an N-terminal palmitoylation motif. Having one end fixed could provide a significant restriction on the accessible conformations because the N and C termini can no longer cross paths. To examine the effect of surface attachment on conformational dynamics, we replaced the N-terminal palmitoylation motif with a biotinylation site. The resultant biotinylated protein was attached directly to a passivated microscope slide using streptavidin. To prevent interactions with the slide, we used an inert proteolipid surface composed of biotinylated bovine serum albumin followed by the application of a dilute solution of protein-free liposomes. The resulting surface shows extremely low levels of nonspecific binding (supplemental Fig. S2).

We measured smFRET from the same labeling site combinations used in encapsulation studies (Fig. 6). Src phosphorylation was carried out in solution after fluorescent labeling but before immobilization. Similar effects on smFRET were observed when Src (along with ATP and Mg^{2+}) was added to immobilized protein in the sample chamber (data not shown). When CTD2 is surface-immobilized, the shift induced by phosphorylation is much more apparent (*solid curves,* Fig. 6*A*). The entire distribution shifts visibly toward low FRET. In contrast to the encapsulated samples, all constructs showed a statistically significant shift in median FRET efficiency (Table 4). Immobilization of CTD2 appeared to magnify the effectiveness of phosphorylation as a signal by further separating the two states. As expected, NRB-1 remained the exception with a narrow FRET peak, with no FRET shift upon phosphorylation and no FRET transitions.

Transitions were unaffected by tethering (data not shown). Surprisingly, it is the unphosphorylated state that is most affected by N-terminal tethering (Tables 2 and 4). Surface immobilization had no effect on median smFRET after phosphorylation although smFRET before phosphorylation shows a trend toward higher FRET values. This suggests that the immobilized protein is initially more compact but extends to the

TABLE 1
Location of cysteine residues used in FRET studies

Construct	Labeling sites	Separation (amino acids)
N2B-1	s1273c, s1288c	15
N2B-2	C1394, s1477c	83
N2B-3	s1353c, C1453	100
N2B-4	s1273c, C1394	121
N2B-5	s1353c, s1477c	124
N2B-6	s1323c, C1453	130
N2B-7	s1273c, s1413c	140
N2B-8	s1273c, C1445	172

TABLE 2
Effect of Src phosphorylation on median smFRET efficiency in encapsulated CTD2

Construct	Unphosphorylated	Phosphorylated	*p* value
N2B-1	0.90 ± 0.075	0.88 ± 0.003	NA[a]
N2B-2	0.64 ± 0.016	0.59 ± 0.042	0.299
N2B-3	0.55 ± 0.034	0.48 ± 0.013	0.084
N2B-4	0.45 ± 0.008	0.36 ± 0.016	0.019
N2B-5	0.49 ± 0.061	0.43 ± 0.013	0.286
N2B-6	0.47 ± 0.051	0.43 ± 0.008	0.319
N2B-7	0.43 ± 0.032	0.40 ± 0.038	0.497
N2B-8	0.38 ± 0.027	0.30 ± 0.015	0.065

[a] NA means not applicable.

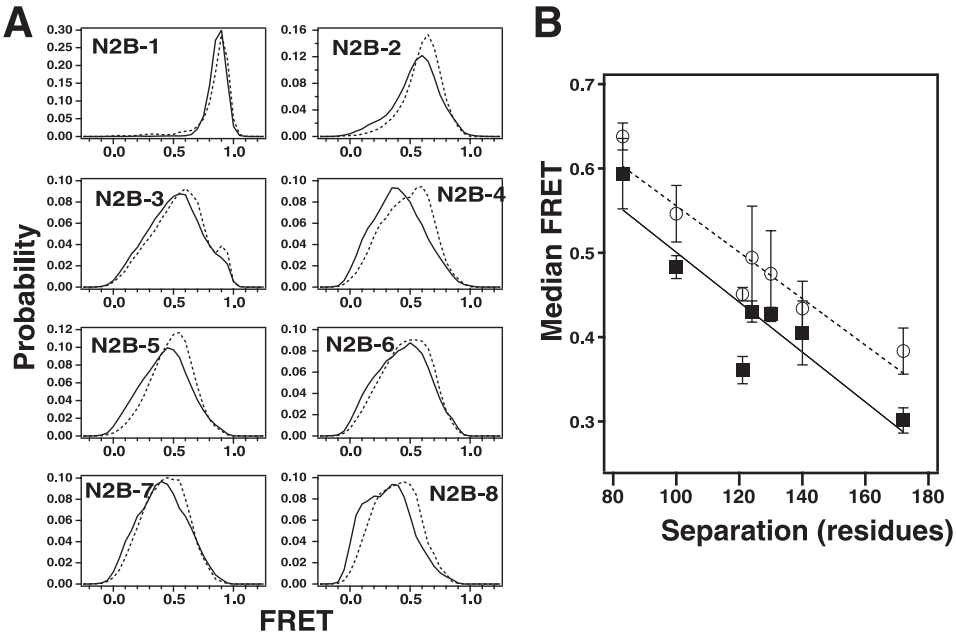

FIGURE 5. **Effect of Src phosphorylation on single molecule FRET in the GluN2B CTD2.** *A,* single molecule FRET was measured for each FRET construct before and after Src phosphorylation. Constructs are shown in order of the fluorophore separation as indicated in each panel. The *histogram* contains FRET values calculated for each 100-ms frame of observation. Unphosphorylated proteins are shown as *dashed lines*. Phosphorylated proteins are shown as *solid lines*. *B,* median FRET for each distribution above plotted against the fluorophore separation in residues. Data were fit to a line using nonlinear least squares fitting. Unphosphorylated proteins are shown as *open circles* fit to a *dashed line*. Src-phosphorylated proteins are shown as *filled squares* fit to a *solid line*. *Error bars* are from replicate measurement of median FRET in separate experiments.

same extent after phosphorylation. The linear relationship between FRET efficiency and fluorophore separation in the primary sequence was preserved in immobilized samples indicating a lack of local structure (Fig. 6*B*).

DISCUSSION

The intracellular domain of GluN2B is so essential to receptor function that genetic deletion of the C terminus is lethal (5). Although the CTD is intrinsically disordered, it exerts allosteric effects on receptor gating and trafficking that are modulated through Src phosphorylation, which alters both channel currents and receptor trafficking (14). To understand how tyrosine phosphorylation regulates NMDAR, we characterized the effect of Src phosphorylation on the conformation and dynamics of the C-terminal domain from the NMDA receptor subunit GluN2B.

This study used a fragment (CTD2) that contains the two major Src phosphorylation sites (Fig. 1). All ensemble methods confirm that CTD2 is intrinsically disordered under physiological buffer conditions. This agrees with predictions based on amino acid sequence (Fig. 1*B*). The protein is rapidly degraded during proteolysis experiments (Fig. 2). The appearance of higher molecular weight intermediates during digestion suggests the existence of a protein "core" that contains aromatic residues. This agrees with the SEC data, which show that CTD2 is more compact than a random coil. CTD2 is a compact disordered globule with no stable secondary structure (Fig. 3).

To probe the conformation of CTD2, we used single molecule FRET. This necessitates the use of covalently attached fluorophores that are charged and aromatic. It is inconceivable that the dyes do not participate in the conformational equilibrium, an unavoidable problem associated with using exogenous probes to study biomolecules. Fluorescent labeling had minimal effects on the radius of hydration particularly when compared with the much smaller phosphate moiety. This speaks to the powerful specific activity of this post-translational modification.

We placed FRET pairs throughout the protein to probe for local structure. If local structure existed, we would have expected a dispersion of FRET values (37). Instead, the results

TABLE 3

Effect of Src phosphorylation on the percent of molecules showing stochastic FRET transitions

Construct	Unphosphorylated	Phosphorylated
	%	%
N2B-1	3 ± 4	1 ± 1
N2B-2	52 ± 18	62 ± 10
N2B-3	75 ± 6	80 ± 3
N2B-4	87 ± 1	85 ± 0
N2B-5	81 ± 3	93 ± 4
N2B-6	81 ± 5	88 ± 6
N2B-7	81 ± 7	91 ± 1
N2B-8	84 ± 1	83 ± 9

TABLE 4

Effect of Src phosphorylation on median smFRET efficiency in surface immobilized CTD2

Construct	Unphosphorylated	Phosphorylated	*p* value
N2B-1	0.92 ± 0.011	0.90 ± 0.013	NA[a]
N2B-2	0.65 ± 0.006	0.55 ± 0.005	0.003
N2B-3	0.64 ± 0.015	0.45 ± 0.023	0.010
N2B-4	0.50 ± 0.010	0.37 ± 0.038	0.045
N2B-5	0.57 ± 0.036	0.43 ± 0.005	0.033
N2B-6	0.57 ± 0.045	0.42 ± 0.013	0.044
N2B-7	0.45 ± 0.030	0.35 ± 0.0002	0.041
N2B-8	0.40 ± 0.029	0.27 ± 0.030	0.047

[a] NA means not applicable.

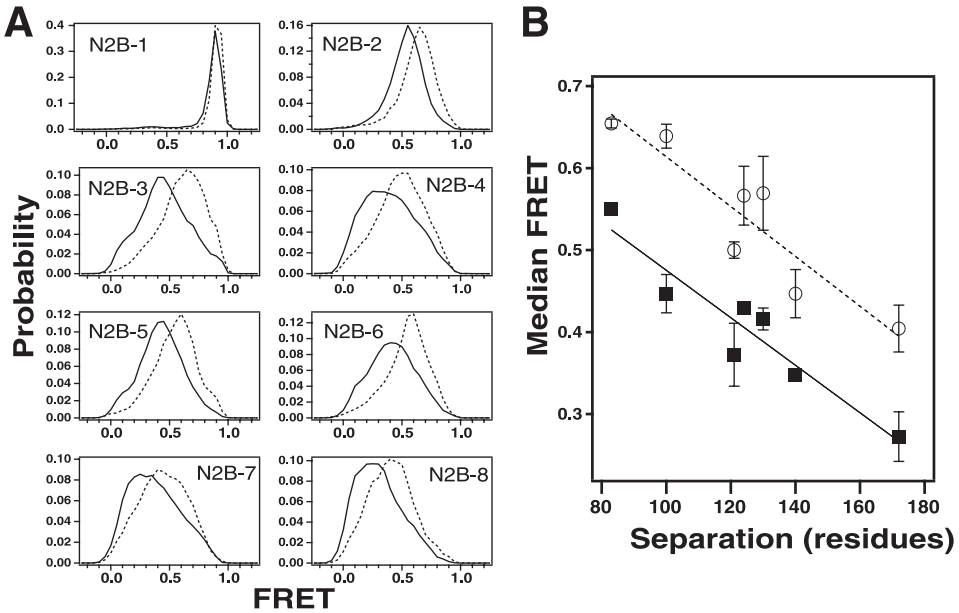

FIGURE 6. **Effect of surface tethering on phosphorylation-induced conformational changes in the GluN2B CTD2.** For these experiments, the palmitoylation sites in the N terminus of CTD2 were replaced with a biotinylation sequence, which allows for directional tethering of CTD2 to a passivated microscope slide. All labeling sites for FRET were identical to the previous experiments. *A,* single molecule FRET was measured for each FRET construct before and after Src phosphorylation. Constructs are shown in order of the fluorophore separation as indicated in each panel. The *histogram* contains FRET values calculated for each 100-ms frame of observation. Unphosphorylated proteins are shown as *dashed lines*. Phosphorylated proteins are shown in as *solid lines*. *B,* median FRET for each distribution above plotted against the fluorophore separation in residues. Data were fit to a line using nonlinear least squares fitting. Unphosphorylated proteins are shown as *open circles* fit to a *dashed line*. Src-phosphorylated proteins are shown as *filled squares* fit to a *solid line*. *Error bars* are from replicate measurement of median FRET in separate experiments.

showed minimal positional dependence and instead the FRET scaled linearly with the fluorophore separation. Such statistical scaling is a general property of random coils and suggests a lack of discernible, stable conformations or local structure in the native state ensemble. The protein is truly "molten" sampling a random distribution of states albeit with some component on a slow time scale.

The smFRET distributions were irregularly shaped with some positional variability that was reproducible. The shape of the point wise smFRET distribution depends on both the FRET states visited and the duration of each FRET state. Thus, changes in conformation *or* the lifetime of individual states would change the shape. It is difficult to interpret changes in the distribution shape, so we only extracted the median FRET because the distributions had a clear predominant peak.

Both the ensemble and single molecule data suggest that phosphorylation results in a general expansion of the polypeptide chain. Median FRET shifted for all constructs regardless of their positioning relative to the phosphorylation sites. Regardless of the phosphorylation state, the FRET scales linearly with amino acid separation. This along with the CD spectra suggest a featureless energy landscape without favored conformations or a stable local structure.

Because GluN2B is palmitoylated in neurons, we examined the effect of surface tethering on the conformation of CTD2. Disordered domains are frequently linked to transmembrane proteins, with unknown effects on their conformation. The surface should reduce the number of accessible conformations through steric repulsion. Such effects are difficult, if not impossible, to measure in solution but can be observed in immobilized single molecules.

The conformation of CTD2 was affected by immobilization with a trend toward higher FRET values (Tables 2 and 4). This suggests that CTD2 becomes more compact when the N terminus is immobilized. In contrast, the FRET values after phosphorylation were unaffected by immobilization so the expanded state appears the same. The net result is a greater net shift upon phosphorylation. Thus, in these experiments, surface tethering amplified the signal induced by phosphorylation by magnifying the difference between states.

Phosphorylation does not induce structure in CTD2, so the effects on NMDA receptor activity must arise from the general expansion. If anything, CTD2 becomes more like a random coil. The volume change could affect steric interactions with the membrane and change the orientation of this domain relative to the ion channel or exert tension on the final transmembrane domain. The proteolysis experiments suggest that the expansion would result in greater surface exposure of potential sites of post-translational modification and protein binding. Such a global rearrangement could change the affinity for protein interactions either with the other NMDA receptor subunits or synaptic proteins like CAMKII or PSD-95.

CTD2 may interact with other portions of GluN2B (*e.g.* CTD1 or intracellular loops) or CTD from the other subunits within a tetrameric receptor. Such interactions could easily change the structure of this "domain" away from what we observe in these experiments. CTD2 in isolation represents a "ground state" at equilibrium under physiological pH and ionic strengths. The effect of such interactions remains to be investigated.

Intrinsically disordered intracellular domains are a common feature of cell surface receptors and channels. Many are similarly regulated by phosphorylation. How such disordered CTD might modulate the activity of their associated proteins is a complete unknown. Our findings here suggest that in GluN2B disorder actually increases, which only deepens the mystery of how the allosteric affects are mediated.

Acknowledgments—We thank Ben Sondergoth and Markus Seeliger for providing purified Src kinase, Daniel P. Raleigh for assistance with circular dichroism, and Suzanne Scarlata for assistance with fluorometry. We benefited from conversations with Nicolas Nassar, Todd Miller, and Rashek Kazi.

REFERENCES

1. Lau, C. G., and Zukin, R. S. (2007) *Nat. Rev. Neurosci.* **8,** 413–426
2. Traynelis, S. F., Wollmuth, L. P., McBain, C. J., Menniti, F. S., Vance, K. M., Ogden, K. K., Hansen, K. B., Yuan, H., Myers, S. J., Dingledine, R., and Sibley, D. (2010) *Pharmacol. Rev.* **62,** 405–496
3. Köhr, G., and Seeburg, P. H. (1996) *J. Physiol.* **492,** 445–452
4. Groc, L., Bard, L., and Choquet, D. (2009) *Neuroscience* **158,** 4–18
5. Cull-Candy, S. G., and Leszkiewicz, D. N. (2004) *Sci. STKE 2004,* re16-
6. Ryan, T. J., Emes, R. D., Grant, S. G., and Komiyama, N. H. (2008) *BMC Neurosci.* **9,** 14
7. Sprengel, R., Suchanek, B., Amico, C., Brusa, R., Burnashev, N., Rozov, A., Hvalby, O., Jensen, V., Paulsen, O., Andersen, P., Kim, J. J., Thompson, R. F., Sun, W., Webster, L. C., Grant, S. G., Eilers, J., Konnerth, A., Li, J., McNamara, J. O., and Seeburg, P. H. (1998) *Cell* **92,** 279–289
8. Kutsuwada, T., Sakimura, K., Manabe, T., Takayama, C., Katakura, N., Kushiya, E., Natsume, R., Watanabe, M., Inoue, Y., Yagi, T., Aizawa, S., Arakawa, M., Takahashi, T., Nakamura, Y., Mori, H., and Mishina, M. (1996) *Neuron* **16,** 333–344
9. Hayashi, T., Thomas, G. M., and Huganir, R. L. (2009) *Neuron* **64,** 213–226
10. Smotrys, J. E., and Linder, M. E. (2004) *Annu. Rev. Biochem.* **73,** 559–587
11. Kornau, H. C., Schenker, L. T., Kennedy, M. B., and Seeburg, P. H. (1995) *Science* **269,** 1737–1740
12. Sans, N., Prybylowski, K., Petralia, R. S., Chang, K., Wang, Y. X., Racca, C., Vicini, S., and Wenthold, R. J. (2003) *Nat. Cell Biol.* **5,** 520–530
13. Kim, E., and Sheng, M. (2004) *Nat. Rev. Neurosci.* **5,** 771–781
14. Chen, B. S., and Roche, K. W. (2007) *Neuropharmacology* **53,** 362–368
15. Moon, I. S., Apperson, M. L., and Kennedy, M. B. (1994) *Proc. Natl. Acad. Sci. U.S.A.* **91,** 3954–3958
16. Xiong, Z. G., Pelkey, K. A., Lu, W. Y., Lu, Y. M., Roder, J. C., MacDonald, J. F., and Salter, M. W. (1999) *J. Neurosci.* **19,** 37RC
17. Yu, X. M., and Salter, M. W. (1999) *Proc. Natl. Acad. Sci. U.S.A.* **96,** 7697–7704
18. Zheng, F., Gingrich, M. B., Traynelis, S. F., and Conn, P. J. (1998) *Nat. Neurosci.* **1,** 185–191
19. Ascher, P. (1998) *Nat. Neurosci.* **1,** 173–175
20. Romero, P., Obradovic, Z., Li, X., Garner, E. C., Brown, C. J., and Dunker, A. K. (2001) *Proteins* **42,** 38–48
21. Dosztányi, Z., Csizmok, V., Tompa, P., and Simon, I. (2005) *Bioinformatics* **21,** 3433–3434
22. Uversky, V. N. (2002) *Eur. J. Biochem.* **269,** 2–12
23. Iakoucheva, L. M., Radivojac, P., Brown, C. J., O'Connor, T. R., Sikes, J. G., Obradovic, Z., and Dunker, A. K. (2004) *Nucleic Acids Res.* **32,** 1037–1049
24. Johnson, L. N., and Lewis, R. J. (2001) *Chem. Rev.* **101,** 2209–2242
25. Garza, A. M., Khan, S. H., and Kumar, R. (2010) *Mol. Cell. Biol.* **30,** 220–230
26. Baker, J. M., Hudson, R. P., Kanelis, V., Choy, W. Y., Thibodeau, P. H., Thomas, P. J., and Forman-Kay, J. D. (2007) *Nat. Struct. Mol. Biol.* **14,**

738–745
27. Mittag, T., Marsh, J., Grishaev, A., Orlicky, S., Lin, H., Sicheri, F., Tyers, M., and Forman-Kay, J. D. (2010) *Structure* **18,** 494–506
28. Mao, A. H., Crick, S. L., Vitalis, A., Chicoine, C. L., and Pappu, R. V. (2010) *Proc. Natl. Acad. Sci. U.S.A.* **107,** 8183–8188
29. Marsh, J. A., and Forman-Kay, J. D. (2010) *Biophys. J.* **98,** 2383–2390
30. Muller-Spath, S., Soranno, A., Hirschfeld, V., Hofmann, H., Ruegger, S., Reymond, L., Nettels, D., and Schuler, B. (2010) *Proc. Natl. Acad. Sci. U.S.A.* **107,** 14609–14614
31. Mittag, T., Orlicky, S., Choy, W. Y., Tang, X., Lin, H., Sicheri, F., Kay, L. E., Tyers, M., and Forman-Kay, J. D. (2008) *Proc. Natl. Acad. Sci. U.S.A.* **105,** 17772–17777
32. Choi, U. B., McCann, J. J., Weninger, K. R., and Bowen, M. E. (2011) *Structure* **19,** 566–576
33. Zhou, H. X. (2010) *Biophys. J.* **98,** L15–L17
34. McCann, J. J., Choi, U. B., Zheng, L., Weninger, K., and Bowen, M. E. (2010) *Biophys. J.* **99,** 961–970
35. Nakazawa, T., Komai, S., Tezuka, T., Hisatsune, C., Umemori, H., Semba, K., Mishina, M., Manabe, T., and Yamamoto, T. (2001) *J. Biol. Chem.* **276,** 693–699
36. Sass, L. E., Lanyi, C., Weninger, K., and Erie, D. A. (2010) *Biochemistry* **49,** 3174–3190
37. McCann, J. J., Zheng, L., Chiantia, S., and Bowen, M. E. (2011) *Structure* **19,** 810–820
38. Sobolevsky, A. I., Rosconi, M. P., and Gouaux, E. (2009) *Nature* **462,** 745–756